



Direct measurement of radiation pressure and circulating power inside a passive optical cavity

RYAN WAGNER,¹ FELIPE GUZMAN,^{2,3} AKOBUJIJE CHIJOKE,¹ GURPREET KAUR GULATI,⁴ MATTHIAS KELLER,⁴ AND GORDON SHAW^{1,*}

¹Physical Measurement Laboratory, National Institute of Standards and Technology, 100 Bureau Drive, Gaithersburg, MD 20899, USA

²German Aerospace Center (DLR), Institute of Space Systems, Bremen, Linzer Str. 1, 28359 Bremen, Germany

³College of Optical Sciences, University of Arizona, Tucson, AZ 85721, USA

⁴Department of Physics and Astronomy, University of Sussex, Falmer BN1 9QH, UK

*gordon.shaw@nist.gov

Abstract: A mechanical force sensor coupled to two optical cavities is developed as a metrological tool. This system is used to generate a calibrated circulating optical power and to create a transfer standard for externally coupled optical power. The variability of the sensor as a transfer standard for optical power is less than 2%. The uncertainty in using the sensor to measure the circulating power inside the cavity is less than 3%. The force measured from the mechanical response of the sensor is compared to the force predicted from characterizing the optical spectrum of the cavity. These two forces are approximately 20% different. Potential sources for this disagreement are analyzed and discussed. The sensor is compact, portable, and can operate in ambient and vacuum environments. This device provides a pathway to novel nanonewton scale force and milliwatt scale laser power calibrations, enables direct measurement of the circulating power inside an optical cavity, and enhances the sensitivity of radiation pressure-based optical power transfer standards.

1. Introduction

The phenomenon of light reflection from a surface links optical power and force. In classical electromagnetism this connection manifests as the radiation pressure force and was first experimentally quantified in the early 1900s with the Nichols radiometer [1]. For a perfect reflector this force is $2P \cdot \cos(\theta) / c$, where P is optical power, θ is angle of incidence, and c is the speed of light in a vacuum. The connection between force and power can be used to build metrological tools that measure optical power from a known force, or that measure force from a known optical power.

In the kilowatt range, radiation pressure has been measured with percent level uncertainties using a calibrated force transducer [2,3]. In the milliwatt range, piconewton forces have been measured with percent level uncertainty using a calibrated optical power [4,5]. In general, large laser powers can be calibrated from force and small forces can be calibrated from laser power with reduced uncertainty compared to traditional approaches.

The connection between optical power and force within an optical cavity has received less attention from the metrological community [6]. For a given incident laser power at the resonance frequency of the cavity, there is a buildup of circulating optical power. For low-loss cavities it is possible to achieve a circulating power enhancement of 10^5 [7]. In linking laser power and force, the primary advantage of using an optical cavity is that the cavity amplifies the force generated on a cavity mirror for a given input power.

The speed of light c is a large deamplification factor. One Watt of optical power will generate a radiation pressure force of approximately 6.7 nN for normal incidence and unity reflectivity. Use of an optical cavity lessens the requirements for equipment like a high-quality-factor force transducer [4] or a multi-Watt laser system [2] for generating measurable

radiation pressure forces. In turn, this reduces the cost and environmental requirements necessary to build metrological tools that link optical power and force. For example, an optomechanical transfer standard based on a force transducer coupled to an optical cavity will have greatly enhanced sensitivity compared to one lacking an optical cavity.

Development of a macroscopic quantum force standard also benefits from the use of optical cavities. Reflection of a single photon causes a change in momentum of $h\nu \cdot 2\cos(\theta)/c$, where h is Planck's constant and ν is optical frequency. This change in momentum leads to a force on the surface that depends on the quantity, direction, and frequency of incident photons. A quantum force standard based on counting photons is feasible as a result of advances in superconducting nanowire photon detectors [8]. However, the force associated with a quantity of photons that can be counted remains extraordinarily small. Detecting 10^7 photons per second at 1550 nm corresponds to a force less than 10^{-20} N. An optical cavity amplifies the force generated per photon on a macroscopic device.

In this paper, we report development of a compact and portable optomechanical device that consists of optical cavities coupled to a force sensor. This device can be used as a force standard if the input power and cavity properties can be calibrated, as a standard for circulating power inside an optical cavity if the force transducer is calibrated, or as a transfer standard for optical power by comparing the device output to a calibrated power meter. The variability of the sensor as a transfer artifact for optical power is less than 2%. The variability of the sensor in measuring circulating power inside the cavity is less than 3%. These uncertainties are similar to existing systems that link optical power and force without a cavity [2–5,9]. However, the addition of an optical cavity to the metrological system enables novel applications that systems lacking a cavity cannot duplicate. Such applications include measuring the optical power inside the optical cavity and amplifying the power from a given light sources as it interacts with the force transducer. The prediction of force within the cavity based on the input power and a measurement of the cavity spectrum is compared to the force measured by the force transducer. These two forces are found to disagree by 20%. Potential sources for this disagreement are analyzed and discussed.

2. Experimental apparatus

As shown in Fig. 1(c), a monolithic fused silica rectilinearly translating flexure system is used as a force sensor. The system consists of a set of 3 parallelogram flexures that are 11 mm by 12 mm by 2 mm in size. The more compliant primary flexure in the center deflects in response to a photon pressure force, and the outer flexures can modulate the cavity length with attached piezo actuators. Fused silica was chosen for its low mechanical loss and low coefficient of thermal expansion. The primary flexure stiffness was calibrated with the added mass method [10] and the thermal method [11]. For the added mass method, a Sartorius ultramicrobalance [12] was used to calibrate test masses in the hundred-microgram range with 1 μ g of uncertainty. The thermal method calibrations were performed at ambient pressure and temperature inside of a closed vacuum chamber to isolate the system from spurious acoustic vibrations. Two fiber optical cavities, shown in Fig. 1(d), are formed between the primary flexure and the secondary flexures. Integrated V-grooves align the optical fibers relative to the flexures. The fibers are fixed in the V-grooves with UV-cure epoxy. The entire fused silica device is frit bonded to a fused silica optical flat and placed on a series of isolation stages and inside of a vacuum chamber for testing.

One of the two fiber cavities is used as an interferometer to measure displacement and the other is used to drive the flexure by modulating the optical power. The cavity mirrors are fabricated through laser machining the end facets of the optical fibers with a CO₂ laser (SYNRAD 48-1 water-cooled). The laser machining is performed in a series of short laser pulses. The fibers are mounted on a software controlled rotatable stage, where each laser pulse is followed by a rotation of the fibers around their axis by a certain angle. The use of

fiber rotation and multiple laser pulses, ensures the formation of a highly symmetric indentation on the surface and therefore low birefringence of the cavity [13].

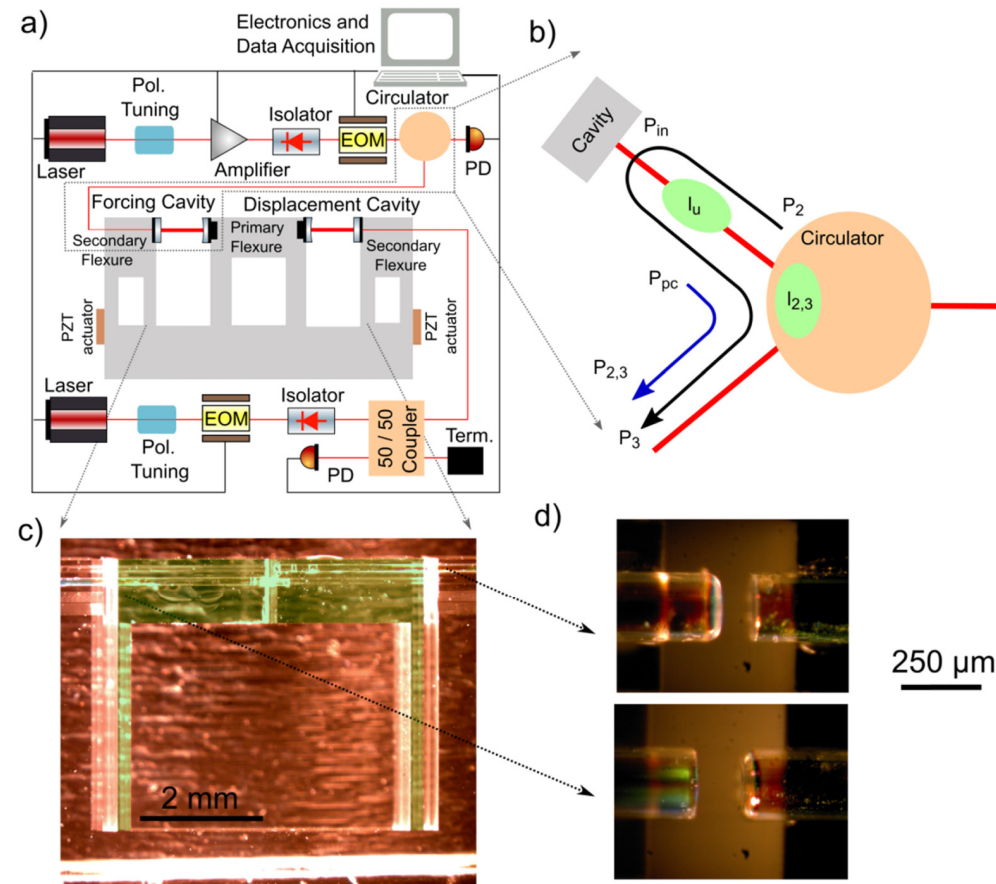


Fig. 1. a) Simplified schematic of optical train and force transducer. Red lines indicate the optical path. b) Final components in optical train before modulation cavity. P_{in} denotes optical power delivered to the fiber leading directly to the optical cavity after the vacuum feedthrough. By breaking the fiber connections and measuring power at P^2 , P_3 , P_{pc} , and $P_{2,3}$ we can calculate the losses l_u and $l_{2,3}$ and in turn calculate P_{in} as indicated in Eq. (13). c) Picture of second flexure, green false color is used to highlight the primary flexure structure. d) Pictures of optical cavities on a flexure.

Multimode fibers are machined to a radius-of-curvature of less than 150 μm , using 100 to 150 laser pulses, each with a duration of around 30 ms and power of 2 W (beam waist of 80 μm). The single mode fibers are laser machined with 3 to 5 laser pulses to form a smooth and uniform flat surface after cleaving. The radius-of-curvature of the machined fibers is measured with a white light interferometer. The optical image of the facet of machined MM-fibers is shown in Fig. 2(a) and the white light interference pattern is shown in Fig. 2(b). From the interference pattern, radius-of-curvature of a particular fiber is extracted. Subsequently, the fiber end facets are coated with a high reflectivity coating of approximately 99.75% reflectivity at 1550 nm (Evaporated Coatings, Inc. # 640).

Each cavity has an independent laser (Newport Velocity TLB-6700) and optical components to deliver light to the cavity. These optical trains are shown in Fig. 1(a). For the forcing cavity optical train, a polarization-dependent, variable optical amplifier (ThorLabs Booster Optical Amplifier) is used to generate the amplitude modulation. Phase electro-optic

modulators (EOMs) are used to apply modulation for the Pound-Drever-Hall (PDH) method [14]. The displacement cavity uses a PDH modulation frequency of 50 MHz and the forcing cavity uses a PDH modulation frequency of 2.9 GHz. Bend insensitive fiber (Nufern 1550B-HP) is used to guide the light through vacuum feedthroughs to the optical cavities. Polarization maintaining fiber is used prior to reaching the phase EOMs, which are the last polarization dependent element in the optical train. The multimode fiber is used for the fiber connection to the second cavity mirror. This fiber is broken shortly after leaving the mirror so no analysis of the transmitted light is possible in the final configuration of the system. The reflected light returns through a circulator or 50/50 coupler to photodiodes. The photodiode signal is demodulated using the EOM signal and the quadrature output sent to a feedback system that tunes the wavelength of the lasers to match the cavity resonance. The amplitude of the flexure response is read by sending the displacement cavity signal to a lock-in amplifier (Zurich Instruments HF2LI) and using the measured PDH slope (see Eq. (3)). The bandwidth of the PDH feedback is much lower than the sensor's mechanical resonance frequency, allowing the dynamic input to the PDH feedback loop to be used as the displacement signal.

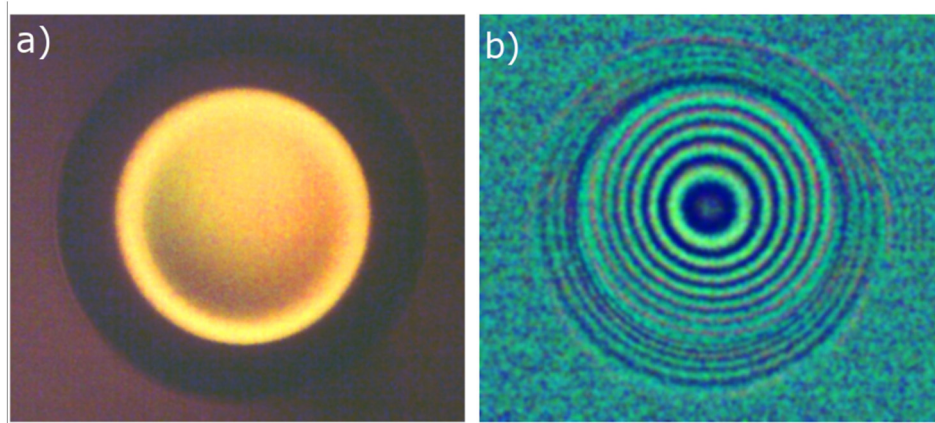


Fig. 2. a) Optical microscope image of the fiber end facet after laser machining. b) White light interferometric image of the end facet. This is used to reconstruct the surface of the laser machined fiber.

3. Theoretical background

Two models are required to describe the system behavior. One is a model of the force transducer response based on measurement of the sensor's mechanical properties and the other is a model of the circulating power based on measurement of the cavity's optical properties.

3.1 A transducer for small optical forces

A high sensitivity force transducer is necessary to detect the optical force on the cavity mirrors. One option is the microcantilever-based forces sensors that are used for atomic force microscopy [15]. However, the force sensitivity of these cantilevers depends on the exact location of the applied force. This effect can be minimized by using a parallelogram flexure, as shown in Fig. 1. This flexure system consists of two flexible cantilevers connected by a rigid element. The rigid element exhibits approximately rectilinear motion, greatly reducing the sensitivity of the force transducer to the location of the applied force [4].

The flexure operates in a resonant, dynamic mode of operation. Resonant operation mechanically amplifies the motional response of the flexure to external forces. Dynamic operation reduces the effect of $1/\omega$ noise and enables the use of lock-in detection to reduce the effect of noise outside of the measurement bandwidth. Assuming the force applied to the

flexure is harmonic, the flexure motion amplitude, A , is well described by a simple harmonic oscillator (SHO) model [16]:

$$A = \frac{A_{sho}}{\sqrt{\left(1 - \left(\frac{\omega}{\omega_0}\right)^2\right)^2 + \left(\frac{\omega}{Q\omega_0}\right)^2}}, \quad (1)$$

where ω is the mechanical drive frequency, A_{sho} is the off-resonance response of the simple harmonic oscillator, ω_0 is the resonance frequency of the flexure, and Q is the quality factor of the flexure. A_{sho} , ω_0 , and Q can be fit from a measurement of A as a function of ω . The amplitude of the harmonic force on the flexure F_{sho} is:

$$F_{sho} = A_{sho} k_L, \quad (2)$$

where k_L is the stiffness of the flexure.

To measure A we used a Fabry-Pérot interferometer and the PDH technique [14]. The interferometer displacement sensitivity measurement for this scheme requires scanning the laser wavelength through the cavity resonance while monitoring the demodulated PDH signal. The amplitude calibration can be expressed as [17]:

$$A = \frac{v_0}{2\Delta\nu \left(\frac{dV}{d\lambda}\right)} V_{pdh}, \quad (3)$$

Where v_0 is the resonance frequency of the cavity, $\Delta\nu$ is the free spectral range (FSR) of the cavity, $\frac{dV}{d\lambda}$ is the slope of the PDH signal near the center frequency of the cavity in units of volts per wavelength, and V_{pdh} is the amplitude of the PDH voltage. To ensure that the measurement of the cavity displacement does not affect the force on the flexure the modulation amplitude is kept small relative to the cavity bandwidth. Additionally, the response of the system as a function of amplitude is observed and our measurements are limited to amplitudes where the system responds linearly.

The stiffness of the flexure k_L can be determined by the added mass (Cleveland) method [10] as:

$$\Delta m = k_L \left(\frac{1}{\omega_0^2}\right) - m_e, \quad (4)$$

where Δm is the added mass, ω_0 is the resonance frequency of the flexure in units of rad/s, and m_e is the equivalent mass of the flexure. By plotting Δm as a function of $1/\omega_0^2$, k_L can be determined as a fit parameter. The stiffness of the flexure can also be determined by the thermal method [11] as:

$$\frac{1}{2} k_b T = \frac{1}{2} k_L \langle x^2 \rangle, \quad (5)$$

where k_b is Boltzmann constant, T is temperature, and $\langle x \rangle^2$ is mean squared deflection. In practice $\langle x \rangle^2$ is found from the area under the power spectral density resonance peak in question.

3.2 Model for circulating power inside an optical cavity

The flexure system we have used as a force transducer is several millimeters in size. Optical fibers are a convenient tool for forming an optical cavity and delivering light at this scale. However, the determination of circulating power inside a fiber based optical cavity is complicated by the mode matching of the fiber mode to the cavity mode.

The optical power circulating in the sensor's fiber Fabry-Pérot cavity (FFPC) is given as [17–19]:

$$P_c = P_{in} \left| \eta_{dip} \right| \left| \frac{i}{1 - g_{rt} e^{i\phi}} \right|^2, \quad (6)$$

where η_{dip} is a parameter representing the depth of the dip in reflected power signal at resonance, g_{rt} is the round-trip cavity gain, P_{in} is the power incident on the first cavity mirror, and ϕ is the nondimensional optical frequency ($\phi = 2\pi(\nu - \nu_0)/\Delta\nu$), ν is the laser frequency, and $i = \sqrt{-1}$. η_{dip} is a parameter that combines of the transmission of the first cavity mirror t_1 and the optical mode matching between the fiber mode and cavity mode α :

$$\eta_{dip} = \alpha^2 t_1^2, \quad (7)$$

Where,

$$\alpha = \int_{S'} \Psi_{cav}^* \Psi_f dS, \quad (8)$$

and,

$$t_1^2 = P_{f,out} / P_{f,in}. \quad (9)$$

Ψ_{cav} is the cavity mode electric field just outside the end of the fiber, Ψ_f is the fiber mode electric field in the same plane, S' is the cross-sectional area, $P_{f,in}$ is the power incident on the fiber mirror, and $P_{f,out}$ is the power transmitted though the fiber mirror in the absence of a cavity and the presence of $P_{f,in}$. The cavity round trip gain g_{rt} represents the total loss over one round trip in the cavity such that:

$$g_{rt} = r_1 r_2 l_{cav}, \quad (10)$$

where r_1 is the reflectivity of the first mirror, r_2 is the reflectivity of the second mirror, and l_{cav} represents other cavity losses. g_{rt} is related to the cavity finesse \mathcal{F} as:

$$\mathcal{F} = \frac{\pi \sqrt{g_{rt}}}{1 - g_{rt}}. \quad (11)$$

The power reflected from the Fabry-Pérot cavity P_r is [17–19]:

$$\frac{P_r}{P_{in}} = \left| \beta - \eta_{dip} \frac{g_{rt} e^{i\phi}}{1 - g_{rt} e^{i\phi}} \right|^2, \quad (12)$$

from which we can fit both η_{dip} and g_{rt} by measuring P_r as a function of ϕ . β is the mode matching between the directly reflected light and the fiber mode. We will assume that $\beta = 1$. This is reasonable for a thin, flat input mirror. We have also assumed that the input mirror reflectivity is close to one. Use of Eq. (12) allows calculation of circulating power in the cavity without specific knowledge of t_1 , α , r_1 , r_2 , and l_{cav} .

The power incident on the first cavity mirror P_{in} needs to be determined. Because we are using a fiber-based system we cannot measure P_{in} directly. Instead we must infer P_{in} from measurements made elsewhere in the optical path. The final part of the optical train before the cavity consists of optical fiber, a vacuum feedthrough, and a circulator. To calculate P_{in} we disconnect the optical train and measure power at the locations indicated in Fig. 1(b). P_{in} is then given as:

$$P_{in} = \left(\frac{P_{pc} P_3}{P_{2,3} P_2} \right)^{\frac{1}{2}} \left(\frac{P_2}{P_{pd}} \right) P'_{pd} \quad (13)$$

where P_{pd} is the power on a permanently connected photodiode during the input power calibration procedure and P'_{pd} is the power on this photodiode during the experiment.

There are a few important assumptions implicit in Eq. (13). First, we have assumed that when we connect and disconnect FC/APC connectors for the purposes of measuring power we do not change the loss characteristics of the connection. It is reasonable to assume that there are no significant such changes if the connector ends are not damaged or contaminated. Measurement of transmitted power through one of the connectors is stable at the percent level after repeated disconnections. Second, we have neglected light reflected from the end of the FC/APC connectors. Third, we have assumed that the FC/APC connection between the second port of the circulator and the vacuum feedthrough is equivalent to the connection between the laser patch cable and the second port of the circulator for the purposes of characterizing $l_{2,3}$. Finally, we have assumed that β is equal to one. We estimate that these assumptions contribute 5% standard uncertainty to each of the powers measured during this procedure.

Finally, we can convert the calculated circulating power inside the cavity P_c into force F_{fpc} as:

$$F_{fpc} = \frac{2P_c}{c}, \quad (14)$$

where we assume negligible mirror loss and normal incidence.

4. Results and discussion

Force predicted from circulating power and radiation pressure (Eq. (6) and Eq. (14)) has been compared to force measured by the force transducer (Eq. (1) and Eq. (2)) for 2 different flexure optical cavity systems and a total of 18 experimental repeats. Sixteen of these were in air and two of these were under vacuum. Parameters that should not affect the agreement between the two force measurements, such as the choice of optical resonance, cavity optical mode, AC and DC input power, input loss, etc. are varied. One experiment comprises

characterization of the optical cavities by scanning the laser frequency with and without optical phase modulation. Short-range cavity wavelength sweeps across one cavity resonance are repeated approximately 100 times each experiment to generate statistics of our measured cavity properties. Long range wavelength sweeps across several cavity resonances are done twice and used to determine the FSR.

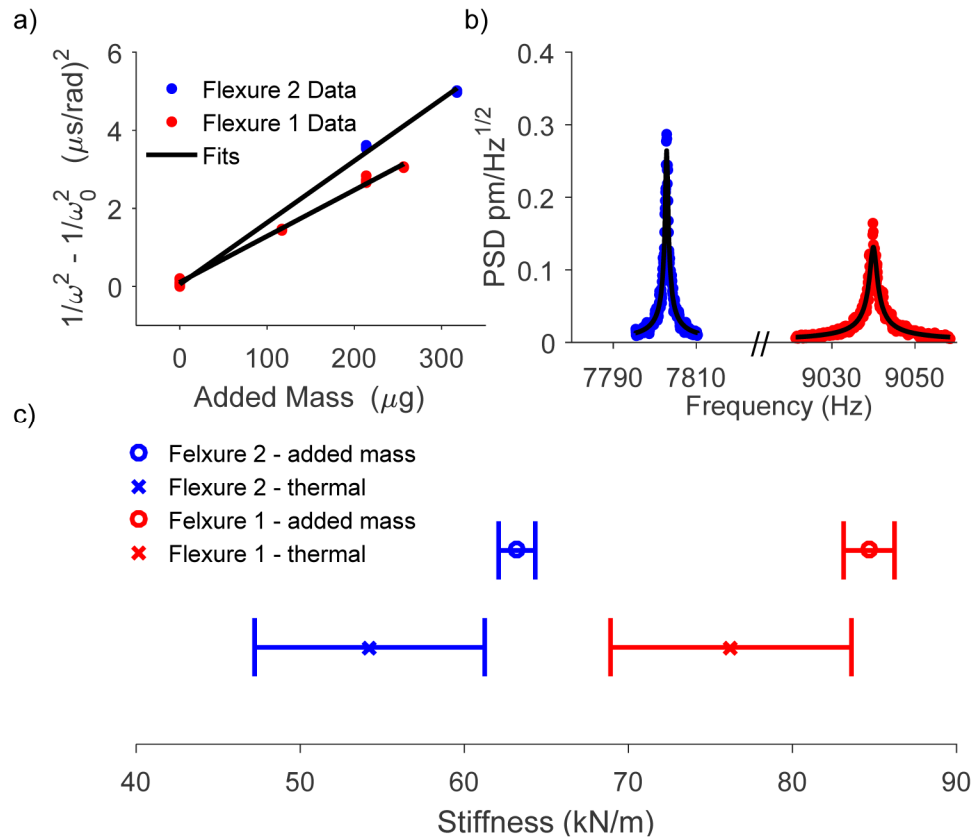


Fig. 3. Flexure calibration. Both the added mass method and thermal method were used to calibrate the flexures; representative calibration data is shown in (a) and (b), respectively. The results of these calibration are shown in (c): $k_L = (84.7 \pm 1.6)$ kN/m for the first flexure added mass method, $k_L = (63.2 \pm 1.1)$ kN/m for the second flexure added mass method, $k_L = (76.3 \pm 7.3)$ kN/m for the first flexure thermal method, and $k_L = (54.2 \pm 7.0)$ kN/m for the second flexure thermal method.

Figure 3 shows the results of flexure stiffness calibration with both the added mass method (Eq. (4)) and the thermal method (Eq. (5)). The stiffness measured with the thermal method is systematically lower than the stiffness measured with the added mass method. This is likely caused by imperfections of the isolation of the flexure from additional sources of environmental noise. The flexure is particularly sensitive to vibrations transmitted through the air. Opening the vacuum chamber housing the device results in an order of magnitude increase in the measured mean squared deflection at the resonance peak. For this reason, the stiffness from the added mass method is used in the analysis. However, the thermal method remains appealing as a built-in calibration tool for an optomechanical force transducer and a reliable thermal method calibration could likely be achieved by better isolation of the flexure from the surrounding environment and a redesign of the flexure to minimize the influence of ambient acoustic noise.

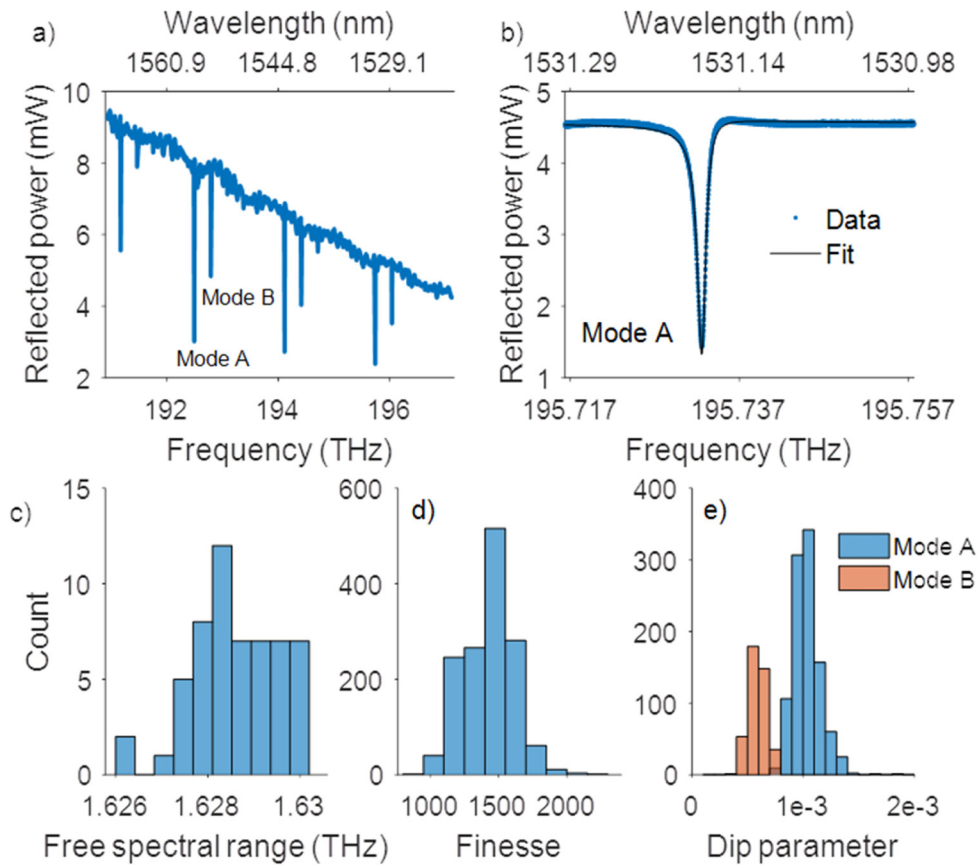


Fig. 4. Characterization of the fiber Fabry-Pérot cavity. a) long range wavelength sweep, b) short range wavelength sweep, c) FSR, d) finesse, e) η_{dip} (i.e dip parameter). The finesse, free spectral range, and the magnitude of the dip parameter was measured in order to calculate the cavity circulating power.

Figure 4 shows the results of fitting the reflected power spectrum to Eq. (12). This fit determines the parameters necessary to calculate the circulating power inside the cavity with Eq. (6). Figure 4(a) shows a representative long-range wavelength sweep over several cavity resonances. The long-range variation of the background signal as a function of wavelength is caused by the wavelength dependence of our optical amplifier. The short-range variation of the background signal is either due to parasitic cavities or from wavelength dependent polarization fluctuations passing through polarization dependent optical elements. There are two distinct transverse optical modes. Optical mode A has an $|\alpha|^2$ of approximately 0.5 and optical mode B has an $|\alpha|^2$ of approximately 0.3. These mode matching factors are calculated using Eq. (7), the fit value of η_{dip} , and the independently measured transmission of the input fiber mirror which was $t_1^2 = (1.968 \pm 0.44) \times 10^{-4}$ at 1550 nm (all uncertainties are reported as one standard deviation). Both optical modes at different axial mode numbers were analyzed. Figure 4(b) shows a representative short-range wavelength sweep over a single optical resonance. The effect of short-range variations of the background signal has been minimized by fitting a 4th order polynomial to the background near the resonance peak and dividing it out. There is some small asymmetry in the reflected power spectra that is fit by allowing η_{dip} to be complex. It appears that the effect of the asymmetry on our data is subtle,

in that the real and complex curve fits do not lead to significantly different values of P_c . However, it may be possible to obtain some extra information from the asymmetry about the cavity alignment and mode matching [18] to aid in cavity assembly in future work.

Figure 4(c) shows the histogram of all measured free spectral range values for the second flexure. The free spectral range is measured to be (1.6286 ± 0.0009) THz. Figure 4(d) shows the histogram of all fitted finesse values. The finesse value taken across all short-range wavelength sweeps is 1430 ± 182 . This distribution is approximately Gaussian with a skewness of 0.0269 and a kurtosis of 2.987. Figure 4(e) shows the histograms of the fitted magnitude of η_{dip} . The two distributions correspond to the two different optical modes examined in the optical cavities coupled to flexure 2.

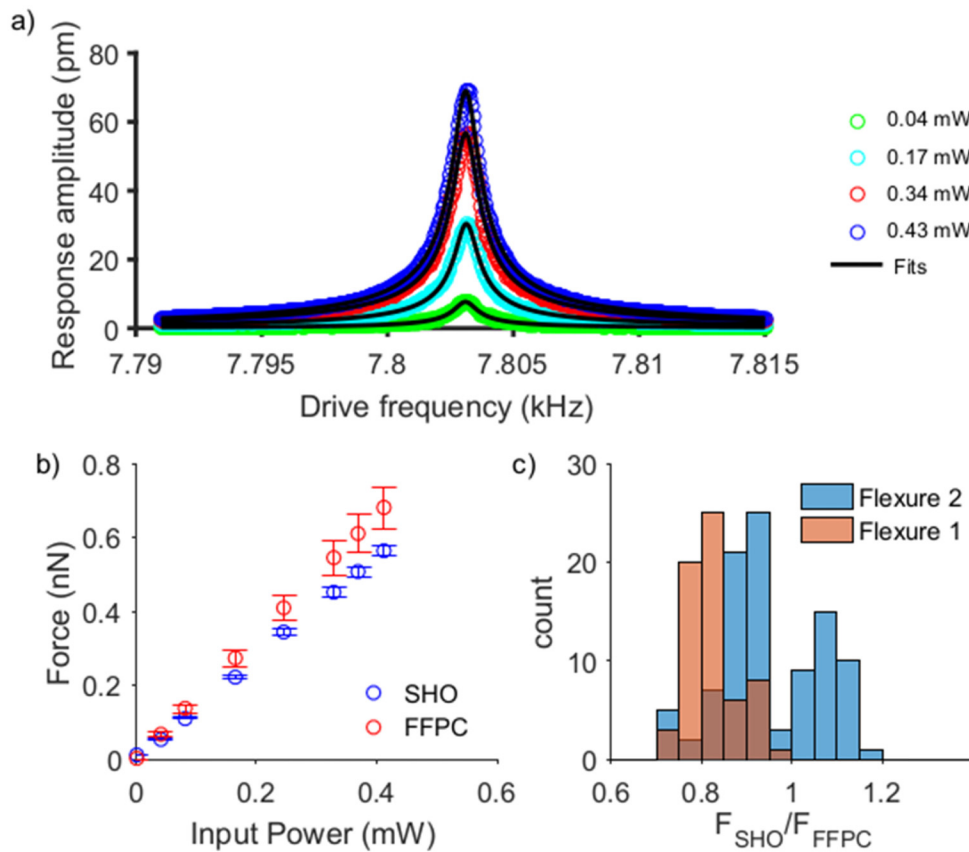


Fig. 5. a) The response of the flexure as drive amplitude signal and drive frequency of the modulating input laser power is varied. b) A comparison of the force calculated from the flexure response (SHO) and the force calculated from the radiation pressure equation (Eq. (14)) and the fiber Fabry-Pérot cavity model (FFPC). c) A statistic comparison of the agreement between the two applied models.

The flexure mechanical response to four different drive amplitudes is shown as a function of drive frequency in Fig. 5(a). This data is fit with Eq. (1), and combined with the flexure stiffness allows us to measure the force on the cavity mirror. The maximum flexure response was approximately 80 pm. Figure 5(b) compares force from Eq. (2) and force from Eq. (14) for a representative experiment on the second flexure for eight different drive amplitudes. For this example, the maximum generated force is on the order of a nanonewton and the two models are close in the value of predicted force, but not in exact agreement.

Table 1 shows the breakdown of uncertainty for a single experiment. The values and uncertainties of the force from the force transducer, the calculated circulating power inside the cavity, and the ratio of the compared force values are shown. The dominant contributions to the uncertainty in the force transducer are the flexure stiffness and the interferometer calibration. The dominant contribution to the uncertainty in the circulating power is the input power into the cavity. The uncertainties of parameters that have been measured multiple times in a single experiment have been averaged to reduce their contribution to the final uncertainty. For the example shown in Table 1, the uncertainty breakdown suggests that the models do not agree, thus there is likely either additional uncertainty or additional physics that is not captured by this analysis.

Table 1. A representative uncertainty analysis of one data point in one experiment on flexure 1. The flexure force, circulating power, and force ratio are combined standard uncertainties. Input variables have been averaged to reduce uncertainty in cases where we do not expect the measurand to vary. All uncertainties are reported as one standard deviation or one standard deviation of the mean as appropriate. The uncertainty in flexure stiffness arises from the uncertainty in fitting Eq. (4). The uncertainty in the input power is as described in the input power loss analysis. All other uncertainties are type A uncertainties.

Parameter Name	Expression	Value	Uncertainty contribution
Flexure force	F_{sho}	(506 ± 13) pN	$\frac{dF_{sho}}{dx} S_x$
PDH voltage	V_{pdh}	$(53.2 \pm 0.1) \times 10^{-6}$ V	1.2 pN
Interferometer calibration	$\frac{v_0}{2\Delta v \left(\frac{dV}{d\lambda} \right)}$	(151 ± 3) pm/V	9.4 pN
Flexure Stiffness	k_L	$(6.30 \pm 0.10) \times 10^4$ pN/pm	8.8 pN
Circulating Power	P_c	(91.6 ± 7.6) mW	$\frac{dP_c}{dx} S_x$
Input power	P_{in}	(0.37 ± 0.03) mW	7.6 mW
Dip parameter	$ \eta_{dip} $	(10.465 ± 0.007) $\times 10^{-4}$	0.6 mW
Finesse	\mathcal{F}	1523 ± 7	0.6 mW
Force ratio	$\frac{F_{sho}}{F_{jpc}}$	0.83 ± 0.07	

Figure 5(c) shows a histogram of the ratio of the two force values for all 18 experiments, on both flexures, and for 7 drive amplitudes. The value of F_{sho} / F_{jpc} across all experiments is 0.904 ± 0.110 with a skewness of 0.521 and a kurtosis of 2.39. Generally, the agreement between the two models is within 21%, but there is considerable variation from experiment to experiment as to how close F_{sho} and F_{jpc} are.

The systematic difference between the two force measurements is not very large relative to the run to run variation. However, the agreement between them is not currently sufficient

to validate generating a calibrated force from the properties of the optical cavity and input power as a metrological tool. The experimental data shows the force measured from the harmonic oscillator model is lower than that predicted from measurement of the optical cavity properties. Three explanations for this discrepancy are possible: an additional force that is not accounted for in the model, a power loss that is not accounted for in the model, or a systematic error in the identification of one of the model input parameters.

Some extraneous sources of force can be investigated by comparing the data taken at atmospheric pressure to data taken under vacuum conditions. For the first flexure F_{sho} / F_{fpc} is 0.835 ± 0.056 in air and 0.798 ± 0.040 in vacuum. These two values are not significantly different given the observed experimental variability. Additionally, fused silica is an excellent thermal insulator and the loss of cavity mirrors is low. These observations suggest that thermal and radiometric effects do not contribute appreciably to the measured forces as these would differ between air and vacuum. We note the ability to perform these experiments at atmospheric pressure reduces the experimental cost and enhances the system portability. Another source of extraneous force could be parasitic capacitance between the primary and secondary flexures. However, because the amplitude of the flexure motion is small relative to the distance between the flexures any force arising from parasitic capacitance will be small when compared to the radiation pressure forces.

One possibility of unaccounted power loss is the parameter β from Eq. (12). We have assumed that β is one. The largest effect of β less than one is a misidentification of P_{in} . In the power input loss analysis, we assumed that all of the observed loss occurred inside the optical train. Power loss associated with β is fundamentally different as this power loss impinges on the first cavity mirror and therefore should not be subtracted from P_{in} . From the available observations we cannot independently determine β . Calculations of β for accounting for the finite thickness of the fiber mirror stacks as well as damage from the laser machining of the fibers suggest a value of 0.97. However, there is a considerable amount of uncertainty in this number as the properties of the interface region are not well known. Reducing β to a value of 0.95 changes F_{sho} / F_{fpc} to a value of 0.859 ± 0.105 , increasing the difference between the results of the two models. Allowing β to be complex has no effect on the model agreement. Thus, misidentification of β is not the dominant source of discrepancy.

To better understand the effects of the other model input parameters we have examined model agreement as a function of different input parameters to search for correlations. Mode matching, input power, input loss factor, environmental pressure, and cavity resonance wavelength appear uncorrelated with respect to model agreement. Cavity finesse on the second flexure appears to be negatively correlated with model agreement, as shown in Fig. 6. Some of the difference between the two forces is likely connected to our ability to accurately measure the cavity finesse. Our finesse value comes from fitting Eq. (12) to the reflected power as a function frequency to get g_{rt} and using Eq. (11) to convert g_{rt} into finesse. The reflected power is measured on a photodiode and the frequency comes from the calibration of the laser controller. The laser controller frequency output is smoothed to remove noise. A more accurate measurement of cavity finesse, perhaps with a frequency comb or wavemeter to measure wavelength, may minimize the potential for experimental error. The variation in measured finesse is large enough to account for the difference between F_{SHO} and F_{FPC} . By estimating the relative changes in P_c calculated using Eq. (6) and Eq. (11) for the ranges of finesse shown in the data of Fig. 6, it can be shown that the range of finesse values measured are potentially large enough to explain the discrepancy.

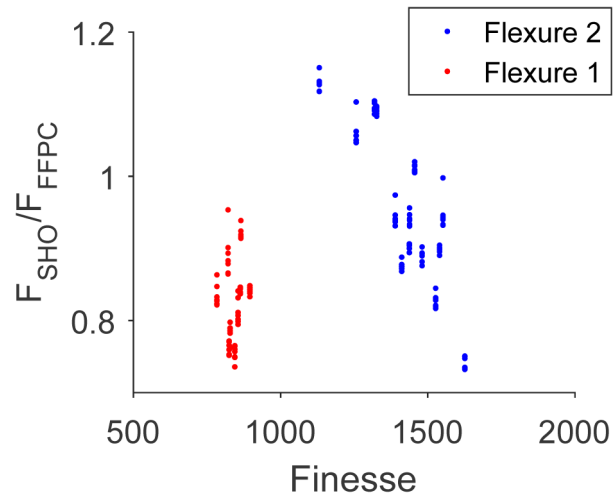


Fig. 6. Correlation between the measured cavity finesse for the two applied modes of force. The negative correlation on the second flexure could indicate that some of the observed disagreement between the two models is connected to unaccounted-for effects in our measurements of the cavity finesse.

Despite the force discrepancy, the cavity optomechanical system is stable enough to be used as a transfer standard for measuring modulating laser power. Figure 7 shows calibration curves for modulating input power on the cavity as a function of the flexure response A_{sho} as fit from Eq. (1). The slopes of these calibration curves are (0.094 ± 0.002) mW/fm for flexure 2 mode B, (0.045 ± 0.002) mW/fm for flexure 2 mode A, and (0.107 ± 0.001) mW/fm for flexure 1. The data for a given flexure and optical mode were taken over a period of several months and the slopes did not change significantly during this time. The calibration curves in Fig. 7 were created using the power input loss calibration relationship described by Eq. (13), and are therefore limited by the same uncertainties. However, by comparing flexure response to a calibrated power meter across a stable optical train a transfer standard limited only by the statistics of the flexure response can be realized.

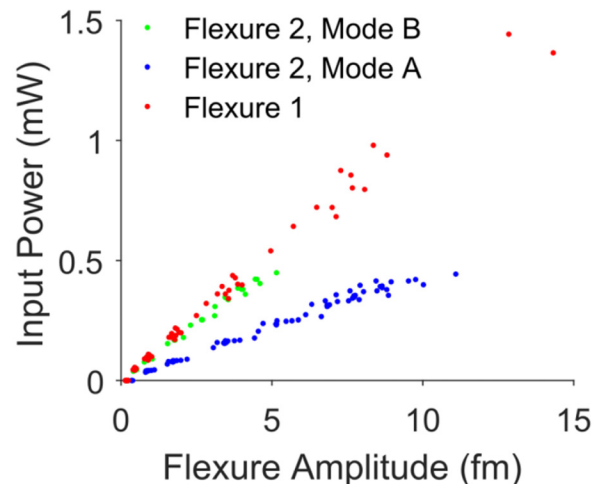


Fig. 7. Calibration curves for using the system as a power meter. The y-axis is the input power and the x-axis is the amplitude obtained by fitting a harmonic oscillation to the signal (A_{sho}).

As a transfer standard this device provides an alternative to an electrical sensor such as a photodiode or thermopile for measuring optical power. Such a transfer standard is useful in environments where it is inconvenient to use traditional electrical sensors, for example in presence of large electric or magnetic fields. Use of the device as an optomechanical power meter also enables the light to be used after it has been measured, although care must be taken in understanding where the light goes after interacting with the flexure as this depends on cavity impedance and mode matching. Measurement dependence on mode matching is captured by the two different calibration curves shown for the different optical modes on flexure 2. Because the mode matching of the two modes is unequal, the circulating power in the two modes is unequal, and hence the force per given input power is unequal. The device as currently implemented is also limited to measuring modulated laser power and cannot measure DC power. A more compliant flexure design may allow this possibility. The ability to modulate the cavity lengths with the secondary flexures relaxes the requirement for use of a tunable laser. The advantage of using an optical cavity as part of this transfer standard is the enhanced sensitivity that depends on the cavity finesse for a given laser input power and flexure stiffness.

A final application of this device is a direct measurement of circulating power inside the cavity via the radiation pressure force. This measurement is given by using Eq. (1) and Eq. (2) to calculate force and then Eq. (14) to convert this force to a power. The uncertainty in circulating power is less than 3% for this approach. Using radiation pressure to infer circulating power is useful for quantum-optical cavity experiments [20] where knowledge of the circulating power is required.

5. Conclusions

We have made a direct measurement of the force on a cavity mirror with a calibrated force transducer and compared that force to the force from the radiation pressure equation (Eq. (14)) and a model for the circulating power inside the cavity (Eq. (6)). We have found that the model that described the circulating power given the input power and cavity properties is accurate to within 21% for our experimental setup. Potential improvements to this agreement include better characterization of the optical cavity finesse and input power. Additionally, use of the device as a transfer standard and as a direct measurement of circulating power inside the cavity is discussed. As a transfer standard the device provides an alternative to photodiodes and as a direct measurement of circulating power inside a cavity the device is useful to the cavity optomechanics community.

References

1. E. F. Nichols and G. F. Hull, "A Preliminary Communication on the Pressure of Heat and Light Radiation," *Phys. Rev. Ser. I* **13**(5), 307–320 (1901).
2. P. Williams, J. Hadler, F. Maring, R. Lee, K. Rogers, B. Simonds, M. Spidell, M. Stephens, A. Feldman, and J. Lehman, "Portable, high-accuracy, non-absorbing laser power measurement at kilowatt levels by means of radiation pressure," *Opt. Express* **25**(4), 4382–4392 (2017).
3. P. A. Williams, J. A. Hadler, R. Lee, F. C. Maring, and J. H. Lehman, "Use of radiation pressure for measurement of high-power laser emission," *Opt. Lett.* **38**(20), 4248–4251 (2013).
4. J. Melcher, J. Stirling, F. G. Cervantes, J. R. Pratt, and G. A. Shaw, "A self-calibrating optomechanical force sensor with femtonewton resolution," *Appl. Phys. Lett.* **105**(23), 233109 (2014).
5. F. Mueller, S. Heugel, and L. J. Wang, "Femto-Newton light force measurement at the thermal noise limit," *Opt. Lett.* **33**(6), 539–541 (2008).
6. S. Vasilyan, T. Fröhlich, and E. Manske, "Total momentum transfer produced by the photons of a multi-pass laser beam as an evident avenue for optical and mass metrology," *Opt. Express* **25**(17), 20798–20816 (2017).
7. B. Brandstätter, A. McClung, K. Schüppert, B. Casabone, K. Friebe, A. Stute, P. O. Schmidt, C. Deutsch, J. Reichel, R. Blatt, and T. E. Northup, "Integrated fiber-mirror ion trap for strong ion-cavity coupling," *Rev. Sci. Instrum.* **84**(12), 123104 (2013).
8. F. Marsili, V. B. Verma, J. A. Stern, S. Harrington, A. E. Lita, T. Gerrits, I. Vayshenker, B. Baek, M. D. Shaw, R. P. Mirin, and S. W. Nam, "Detecting single infrared photons with 93% system efficiency," *Nat. Photonics* **7**(3), 210–214 (2013).

9. K. Agatsuma, D. Friedrich, S. Ballmer, G. DeSalvo, S. Sakata, E. Nishida, and S. Kawamura, "Precise measurement of laser power using an optomechanical system," *Opt. Express* **22**(2), 2013–2030 (2014).
10. C. P. Green, H. Lioe, J. P. Cleveland, R. Proksch, P. Mulvaney, and J. E. Sader, "Normal and torsional spring constants of atomic force microscope cantilevers," *Rev. Sci. Instrum.* **75**(6), 1988–1996 (2004).
11. J. L. Hutter and J. Bechhoefer, "Calibration of atomic-force microscope tips," *Rev. Sci. Instrum.* **64**(7), 1868–1873 (1993).
12. Certain commercial products are identified in this article in order to describe the experimental procedure adequately. Such identification is not intended to imply recommendation or endorsement by the National Institute of Standards and Technology, nor is it intended to imply that the products identified are necessarily the best available for the purpose.
13. H. Takahashi, J. Morphey, F. Oručević, A. Noguchi, E. Kassa, and M. Keller, "Novel laser machining of optical fibers for long cavities with low birefringence," *Opt. Express* **22**(25), 31317–31328 (2014).
14. E. D. Black, "An introduction to Pound–Drever–Hall laser frequency stabilization," *Am. J. Phys.* **69**(1), 79–87 (2000).
15. G. Binnig, C. F. Quate, and C. Gerber, "Atomic Force Microscope," *Phys. Rev. Lett.* **56**(9), 930–933 (1986).
16. S. S. Rao, *Mechanical vibrations*, ed. 1986: Addison-Wesley Longman, Incorporated.
17. A. E. Siegman, *Lasers*, ed. 1986, Palo Alto, CA: University Science Books.
18. J. Gallego, S. Ghosh, S. K. Alavi, W. Alt, M. Martinez-Dorantes, D. Meschede, and L. Ratschbacher, "High-finesse fiber Fabry–Perot cavities: stabilization and mode matching analysis," *Appl. Phys. B* **122**(3), 47 (2016).
19. A. Bick, C. Staarmann, P. Christoph, O. Hellmig, J. Heinze, K. Sengstock, and C. Becker, "The role of mode match in fiber cavities," *Rev. Sci. Instrum.* **87**(1), 013102 (2016).
20. M. Aspelmeyer, T. J. Kippenberg, and F. Marquardt, "Cavity optomechanics," *Rev. Mod. Phys.* **86**(4), 1391–1452 (2014).